Analyst

PAPER

View Article Online
View Journal | View Issue

Cite this: *Analyst*, 2024, **149**, 5063

Fast and broad-coverage lipidomics enabled by ion mobility-mass spectrometry†

Yuping Cai,[a] Xi Chen,[a,b] Fandong Ren,[a] Hongmiao Wang,[a,b] Yandong Yin[a] and Zheng-Jiang Zhu *[a,c]

Aberrant lipid metabolism has been widely recognized as a hallmark of various diseases. However, the comprehensive analysis of distinct lipids is challenging due to the complexity of lipid molecular structures, wide concentration ranges, and numerous isobaric and isomeric lipids. Usually, liquid chromatography-mass spectrometry (LC-MS)-based lipidomics requires a long time for chromatographic separation to achieve optimal separation and selectivity. Ion mobility (IM) adds a new separation dimension to LC-MS, significantly enhancing the coverage, sensitivity, and resolving power. We took advantage of the rapid separation provided by ion mobility and optimized a fast and broad-coverage lipidomics method using the LC-IM-MS technology. The method required only 8 minutes for separation and detected over 1000 lipid molecules in a single analysis of common biological samples. The high reproducibility and accurate quantification of this high-throughput lipidomics method were systematically characterized. We then applied the method to comprehensively measure dysregulated lipid metabolism in patients with colorectal cancer (CRC). Our results revealed 115 significantly changed lipid species between preoperative and postoperative plasma of patients with CRC and also disclosed associated differences in lipid classes such as phosphatidylcholines (PC), sphingomyelins (SM), and triglycerides (TG) regarding carbon number and double bond. Together, a fast and broad-coverage lipidomics method was developed using ion mobility-mass spectrometry. This method is feasible for large-scale clinical lipidomic studies, as it effectively balances the requirements of high-throughput and broad-coverage in clinical studies.

Received 28th May 2024,
Accepted 20th August 2024

DOI: 10.1039/d4an00751d

rsc.li/analyst

1. Introduction

Lipid metabolism is involved in a wide spectrum of physiological and pathological processes including energy homeostasis, anti-inflammatory responses, and tumorigenesis.[1,2] Dysregulation in the levels of lipids has been widely recognized as a hallmark of various diseases, such as obesity, cardiovascular diseases, and gastrointestinal diseases.[3,4] Lipidomics, aiming to analyze endogenous lipids with a broad-coverage, aids in the comprehensive understanding of biological processes modulated by lipid metabolism.[5,6] However, the comprehensive analysis of distinct lipids has been challenging due to the complexity of lipid molecular structures, wide concentration ranges, and numerous isobaric and isomeric lipids.[7] For example, the isotopologues (M0 *vs.* M2) of lipids in the same lipid class with one double bond difference are usually overlapped in the MS1 measurement. The co-eluted isobars and isotopologues lead to the co-isolation and co-fragmentation of precursor ions, generating contaminated MS/MS spectra and compromising lipid identification in lipidomics.[8] Traditionally, lipidomic analysis based on the chromatographic separation method of LC-MS took around 10–30 minutes or longer to achieve optimal separation and selectivity.[9,10] Efficient methods, such as subcritical fluid chromatography using CO_2 as the mobile phase, enabled ultra-fast separation of specific lipids such as estrogen and androgen steroids within 1–3 minutes.[11]

Recently, ion mobility-mass spectrometry (IM-MS) has emerged as a new technology for untargeted lipidomics by improving the separation and peak capacity.[12–14] Ion mobility can rapidly separate ions with respect to the differences in their rotationally averaged surface area through collisions occurring between lipid ions and inert buffer gas under an electric field. Lipids separated by ion mobility can be further identified using collision cross-section (CCS) values based on the molecular structure. This unique feature contributes to the separation of structurally similar lipids that are commonly present in biological samples.[15–19] Previous studies have

[a]*Interdisciplinary Research Center on Biology and Chemistry, Shanghai Institute of Organic Chemistry, Chinese Academy of Sciences, Shanghai, 200032, P. R. China. E-mail: jiangzhu@sioc.ac.cn*
[b]*University of Chinese Academy of Sciences, Beijing, 100049, P. R. China*
[c]*Shanghai Key Laboratory of Aging Studies, Shanghai, 201210, P. R. China*
† Electronic supplementary information (ESI) available. See DOI: https://doi.org/10.1039/d4an00751d

demonstrated that the use of IM-MS provided enhanced peak capacity, improvement of signal-to-noise, and separation of lipid isomers.[12,20] In addition, the use of CCS values to lipidomics workflow significantly improved the accuracy of lipid analysis by comparing the experimental CCS and the reference CCS.[21] The reference CCS values can be accessed through measurements of chemical standards, theoretical calculations, and machine learning-based strategies. In recent years, we and other groups have developed a series of reference CCS databases such as LipidCCS,[22] AllCCS,[16,23] and METLIN-CCS Lipid Database,[24] supporting accurate lipid identifications for lipidomics studies.

Furthermore, integrating IM-MS with LC and tandem MS technology (*e.g.*, LC-IM-MS/MS) enables four-dimensional (4D) untargeted lipidomics analysis, wherein the four-dimensional information on *m*/*z* of MS1, retention time (RT), CCS, and MS/MS spectra can be acquired simultaneously in one analysis.[23,25,26] Importantly, we have recently demonstrated that trapped ion mobility spectrometry (TIMS) hyphenated with the parallel accumulation serial fragmentation (PASEF), in which the first TIMS is used for ion accumulation while the second TIMS is employed for mobility separation before MS1 and MS2 data acquisition, can facilitate the separation of isobaric and isomeric lipids.[8] Also, the TIMS-based PASEF technology has been demonstrated to significantly improve the quality and coverage of MS/MS spectra for untargeted lipidomic analyses.[27] Given the long separation time of LC-MS-based analysis, we therefore attempted to develop a fast IM-MS method dedicated to minimizing the analysis time without compromising on the coverage for lipids.

In this study, we developed a fast LC-IM-MS method towards high-throughput untargeted lipidomic analysis. The method required only 8 minutes for separation and over 1000 lipids were identified and quantified in one analysis for different biological samples. To demonstrate its application for clinical lipidomic studies, we applied the method to comprehensively investigate dysregulation in the lipid metabolism of patients with colorectal cancer (CRC). Our results revealed 115 lipid species that were significantly changed between preoperative and postoperative plasma of patients with CRC. Lipid ontology enrichment analysis showed a significant enrichment in negative intrinsic curvature, mitochondrion, glycerophosphoethanolamines, distinct fatty acid classes, membrane component, and endoplasmic reticulum. Further analysis also disclosed significant differences in the carbon number and double bond for individual lipid classes.

2. Method and materials

2.1 Materials

All lipid standards were purchased from Avanti Polar Lipids (Alabaster, AL, USA) and Sigma-Aldrich (St Louis, MO, USA). Lipid standards were dissolved in either MeOH or MeOH/DCM (v/v = 1 : 1) depending on polarity and solubility. NIST SRM 1950 human plasma was purchased from National Institute of Standards and Technology (NIST, Gaithersburg, MD, USA). LC-MS grade water (H_2O), methanol (MeOH) and HPLC grade dichloromethane (DCM) were purchased from Honeywell (Muskegon, MI, USA). LC-MS grade acetonitrile (ACN) and HPLC grade methyl-*tert*-butyl ether (MTBE) were purchased from Merck (Darmstadt, Germany).

2.2 Clinical sample collection

The clinical samples were obtained from our previous publication.[28] For this study, preoperative (n = 23) and postoperative (n = 23) plasma of patients with CRC were collected and analyzed. Plasma samples were collected from patients with CRC recruited from the Colorectal Surgery Department of Harbin Medical University Cancer Hospital (Harbin, China) with written informed consent. All of the patients were staged according to the Union for International Cancer Control (UICC) pathologic tumor-node-metastasis (TNM) classification system (eighth edition, 2016). This study was approved by the Ethics Committee of the Harbin Medical University Cancer Hospital.

2.3 Sample preparation

Biological samples were extracted with a modified MTBE protocol, as described previously.[29,30] For the preparation of NIST human plasma (SRM 1950) and plasma samples of patients with CRC, 60 μL of plasma was first diluted to 400 μL with water. Then, 960 μL of the extraction solvent (MTBE : MeOH = 5 : 1, v/v) containing 20 μL SPLASH LIPIDOMIX Mass Spec Standard (Catalog No. 330707, Avanti) was added. For the preparation of mouse liver tissue samples, the frozen tissues (~10 mg) were collected in an Eppendorf tube and homogenized with 200 μL of water using the homogenizer (Precellys 24, Bertin Technologies, France). 10 μL homogenized solution was taken out and diluted to 400 μL with H_2O. Then, 960 μL of the extraction solvent (MTBE : MeOH = 5 : 1, v/v) was added. For the preparation of the 293T cell, the cell pellet (~1 × 107 cell per sample) was mixed with water. Then, 960 μL of extraction solvent (MTBE : MeOH = 5 : 1, v/v) was added. The solution was vortexed for 60 s, sonicated for 10 min in a water bath (4 °C) and then centrifuged at 3000 rpm for 15 min (4 °C). Next, 500 μL of the upper organic layer was collected in a new Eppendorf tube. Then, 500 μL of MTBE was added to the left layer for further extraction with vortexing, sonication, and centrifugation, as described previously. The upper organic layer was collected. The re-extraction process was repeated three times in total to ensure high extraction efficient and recovery rate. Finally, the pooled organic layer was evaporated to dryness using a vacuum concentrator at 4 °C. The dried extract was kept at −80 °C and reconstituted with 100 μL of DCM : MeOH (1 : 1, v/v) before analysis.

2.4 LC-TIMS-MS analysis

For the analysis of clinical samples, pooled samples were prepared by mixing aliquots of all the biological samples and used as the quality control (QC) samples. The QC samples were injected at a regular interval (every 12 samples) throughout the assay analysis. After individual QC samples, a blank

sample was introduced. In addition, all biological samples were randomized and placed into the run sequence. All IM-MS data were measured using a UHPLC system (1290 series, Agilent Technologies, USA) coupled to timsTOF Pro equipped with an electrospray ionization (ESI) source (Bruker Daltonics, Bremen, Germany). Lipid separation was performed on a Phenomenex Kinetex C8 column (particle size, 2.6 μm; 50 mm (length) × 2.1 mm (i.d.)) used for LC separation. The column temperature was maintained at 55 °C. Mobile phase A was H_2O/ACN (6 : 4, v/v) with 10 mM $HCOONH_4$, and mobile phase B was IPA/ACN (9 : 1, v/v) with 10 mM $HCOONH_4$. Lipids were eluted at 0.5 mL min^{-1} with a linear gradient of 30% B (0–1.5 min), 30% B to 70% B (1.5–5.0 min), stayed at 70% B (5.0–6.0 min), 70% B to 90% B (6.0–6.1 min), stayed at 90% B (6.1–6.5 min), decreased to 30% B within 0.2 min, and stayed at 30% B for 1.3 min for column equilibrium.

For MS acquisition, the PASEF-DDA scan mode was applied to obtain ions with m/z from 100 Da to 1350 Da and mobility from 0.55 to 1.90 V s cm^{-2}. MS parameters were set as follows: capillary voltage was +4500 V and −4600 V for positive and negative ionization modes, respectively; nebulizer pressure, 2.2 bar; dry gas, 10.0 L min^{-1}; dry temperature, 220 °C; number of PASEF MS/MS scans, 2; ramping time, 100 ms; total cycle time, 0.32 s; charge range, 0–1; absolute threshold, 100 cts; active exclusion was checked, and the former target ions were released after 0.1 min; isolation window, 1.2 Da; collision energy, 40 eV.

2.5 Data processing of the four-dimensional (4D) untargeted lipidomics data sets

Raw data (.d file) were loaded and processed using Met4DX (**https://met4dx.zhulab.cn**).[26] Detailed parameters are provided in ESI Table 1.† For the data processing of the plasma samples of patients with CRC, the raw MS data files and MS2 spectra in .mgf files were organized into one folder and imported into Met4DX using R command lines for data processing. Lipid identification was performed using our developed software tool Lipid4DAnalyzer, which is freely available on the internet (**https://lipid4danalyzer.zhulab.cn/**).[25] CCS match tolerances were set as 2% and 4% (minimum and maximum).

2.6 Lipid quantification

For the quantitative analysis of NIST SRM 1950 human plasma and plasma samples of patients with CRC, nine deuterium-labeled lipids (ESI Table 2†) were used for the quantification of corresponding lipid classes. For each lipid class, we chose the specific adduct form and corresponding deuterium-labeled lipid as the internal standards for quantification. The quantification of lipids was achieved using the peak areas and the concentrations of internal standards (eqn (1)),

$$C_{\text{analyst}} = C_{\text{IS}} \times \frac{A_{\text{analyst}}}{A_{\text{IS}}} \quad (1)$$

where C_{analyst} and C_{IS} represent the concentration of quantified lipid and the internal standard, respectively; A_{analyst} and A_{IS} represent the peak areas of quantified lipid and the internal standard, respectively. The linear dynamic range, LOD, LOQ, and reproducibility were also evaluated for quantification (ESI Table 4†).

3. Results and discussion

3.1 A fast and broad-coverage lipidomics method using LC-IM-MS

The 4D untargeted lipidomics method includes four-dimensional data acquisition and data processing using Met4DX (Fig. 1a). Briefly, a fast LC-IM-MS method combining TIMS separation and the PASEF-based data-dependent acquisition (PASEF-DDA) was used to acquire four-dimensional information on MS1, RT, CCS, and MS/MS spectrum simultaneously. Then, Met4DX, an MS spectrum-oriented bottom-up assembly algorithm that we developed, was modified and tailored for 4D untargeted lipidomics data processing. With the integration of the 4D library-based match and fragmentation rule-based refinement, the strategy enables accurate lipid structural identification and precise quantification for high-throughput 4D untargeted lipidomics studies (Fig. 1a). To optimize a the fast and broad-coverage lipidomics method, we first investigated the performances of LC-IM-MS analyses of NIST human plasma samples with LC separation times of 3, 5, 8, 13 or 18 minutes. For the five gradients tested (3, 5, 8, 13 and 18 minutes), the flow rates were kept at 0.50 mL min^{-1}. In addition, the percentages of mobile phases A and B of individual time points were set as the same. The LC gradients of individual methods are provided in ESI Table 3.† Undoubtedly, the number of detected features increased gradually with a longer separation time. A closer examination of reproducibility also showed an obvious improvement from 3 to 8 minutes and slight increases from 8 to 18 minutes (Fig. 1b). Similarly, as the analysis time increased, the number of identified lipids also increased (Fig. 1c). From the perspective of reproducibility, the 8 minute LC-IM-MS method displayed a higher proportion of lipids with relative standard deviation (RSD) <30% than other tested methods.

In addition, we used the 8 minute LC-IM-MS method to analyze human plasma sample repeatedly with 215 injections. The results demonstrated that this method exhibited high reproducibility regarding mass accuracy, retention time, CCS, and intensity (Fig. 2 and ESI Fig. 1†). For example, TG (18 : 1_18 : 1_18 : 1) showed mass shift <10 ppm, RT shift <3 s, CCS shift <1%, and intensity deviation with RSD 12.9% over the course of 215 sample injections (Fig. 2a–d). More examples are provided in ESI Fig. 1.† The "break" in the ppm shift from the 150$^{\text{th}}$ injection was caused by system reboot, and the continuous data acquisition started from the 151$^{\text{th}}$ injection. Next, we evaluated the reproducibility of all identified 1028 lipids within 215 injections. The results showed in Fig. 2e–g that 98.7%, 96.5%, and 99.7% of the values were detected with high reproducibility of mass shift <5 ppm, RT shift <1 s, CCS shift <1%, respectively. 1000 out of 1028 (97%) lipids displayed high reproducibility of intensity with RSD less than 30%

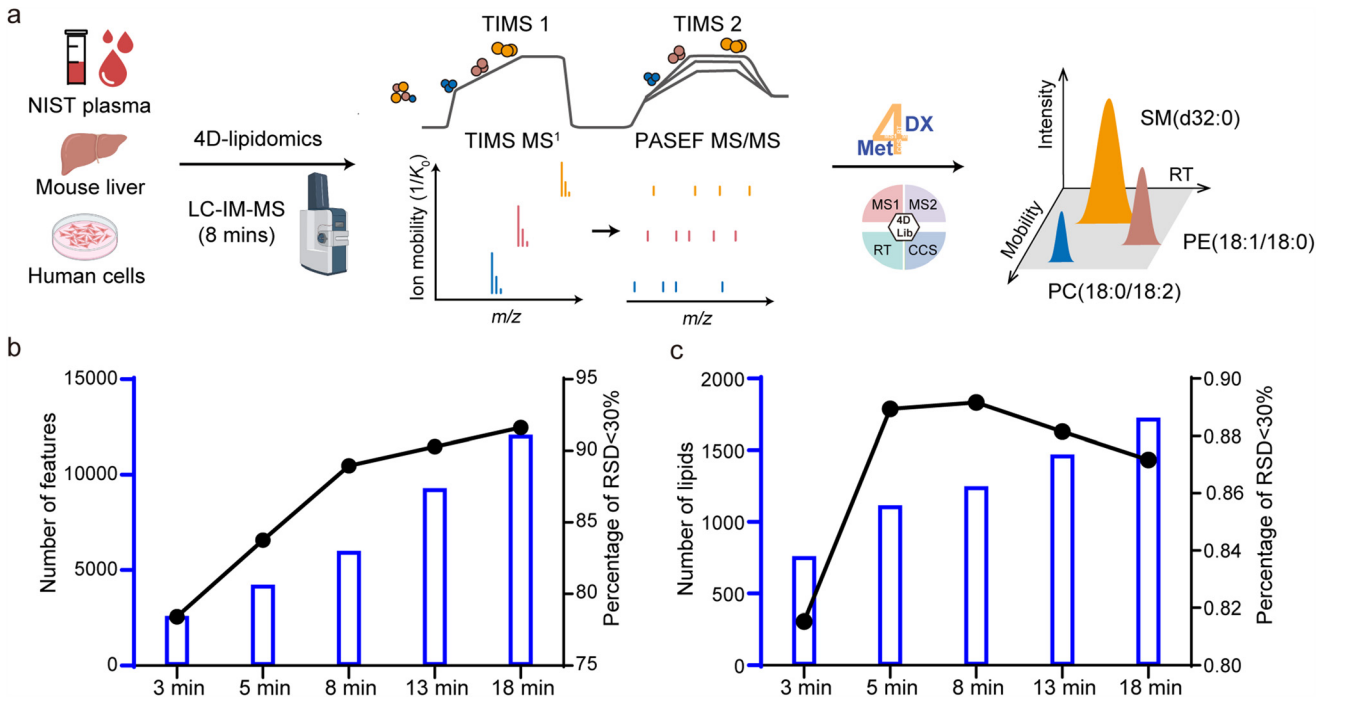

Fig. 1 Development of a fast and broad-coverage four-dimensional (4D) untargeted lipidomics method. (a) Schematic illustration of the 4D untargeted lipidomic analysis includes four-dimensional data acquisition and data processing using Met4DX. (b) The numbers of detected features (blue bar, left *Y* axis) and percentages of features with RSD <30% (black line, right *Y* axis) for LC-IM-MS analyses of NIST human plasma (SRM 1950) samples with separation times of 3, 5, 8, 13, and 18 minutes. (c) The numbers of identified lipids (blue bar, left *Y* axis) and percentages of lipids with RSD <30% (black line, right *Y* axis) for LC-IM-MS analyses of NIST human plasma (SRM 1950) samples with separation times of 3, 5, 8, 13, and 18 minutes. *N* = 6 technical replicates in each analysis.

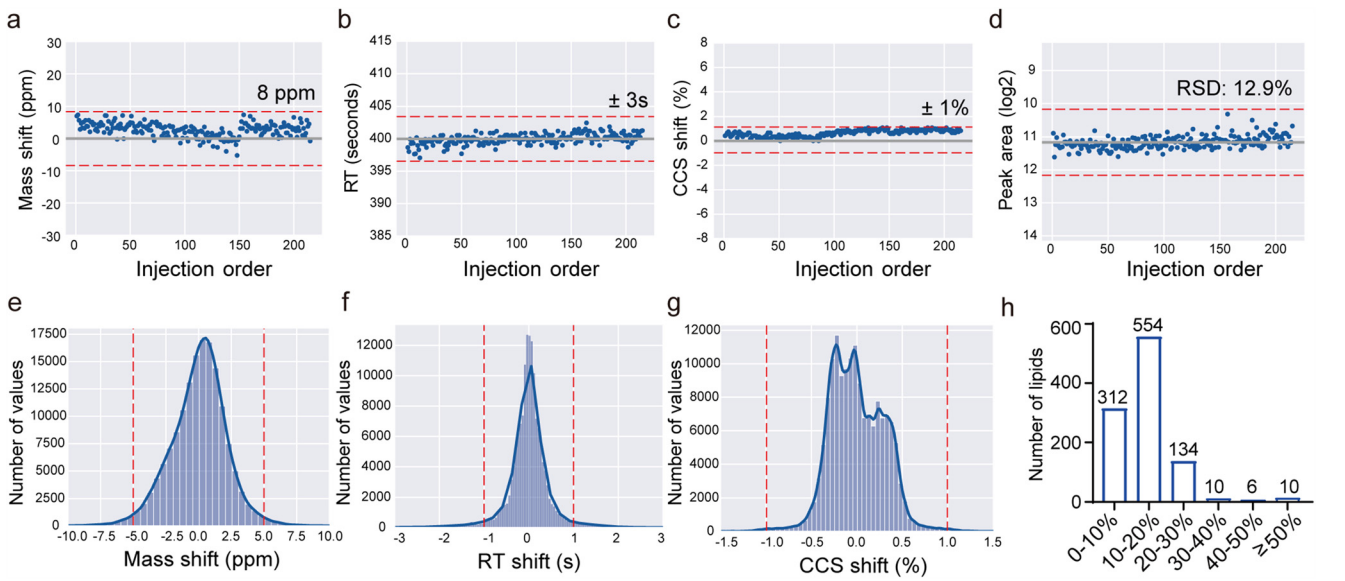

Fig. 2 The fast LC-IM-MS method with high reproducibility of mass accuracy, retention time, CCS value, and intensity. (a–d) Mass shift (a), retention time shift (b), CCS shift (c), and intensity deviation (d) of TG(18 : 1_18 : 1_18 : 1) over 215 sample injections. (e–g) Distribution of mass shift (e), retention time shift (f), and CCS shift (g) of the corresponding values of lipids detected within 215 injections. (h) Bar plots of the RSD distributions of intensities for 1028 lipids detected within 215 injections.

(Fig. 2h). Combined, the above results demonstrate that the 8 minute LC-IM-MS method enables a fast and highly reproducible lipidomics analysis.

The 8 minute LC-IM-MS analysis method demonstrates excellent chromatographic separation and comprehensive coverage of lipids, which is feasible for high-throughput 4D untargeted lipidomics. As the base peak chromatogram (BPC) of the lipid extract from NIST SRM 1950 plasma displays in Fig. 3a, the initial time range eluted polar lipids such as lyso-phospholipids (lysoPLs), monoradylglycerols (MG), sphinganine (Sph), and carnitines (Car). Subsequently, lipids of intermediate polarity, including phospholipids (PLs), diacylglycerols (DG), sphingomyelins (SM), sterols (ST), and ceramides (Cer), were separated and eluted. Finally, highly lipophilic molecules such as cholesteryl esters (CE) and triglycerides (TG) were eluted within 4 to 6 minutes. As a result, over 1000 lipids were measured using the high-throughput 4D untargeted lipidomics approach in one analysis. We also demonstrated the

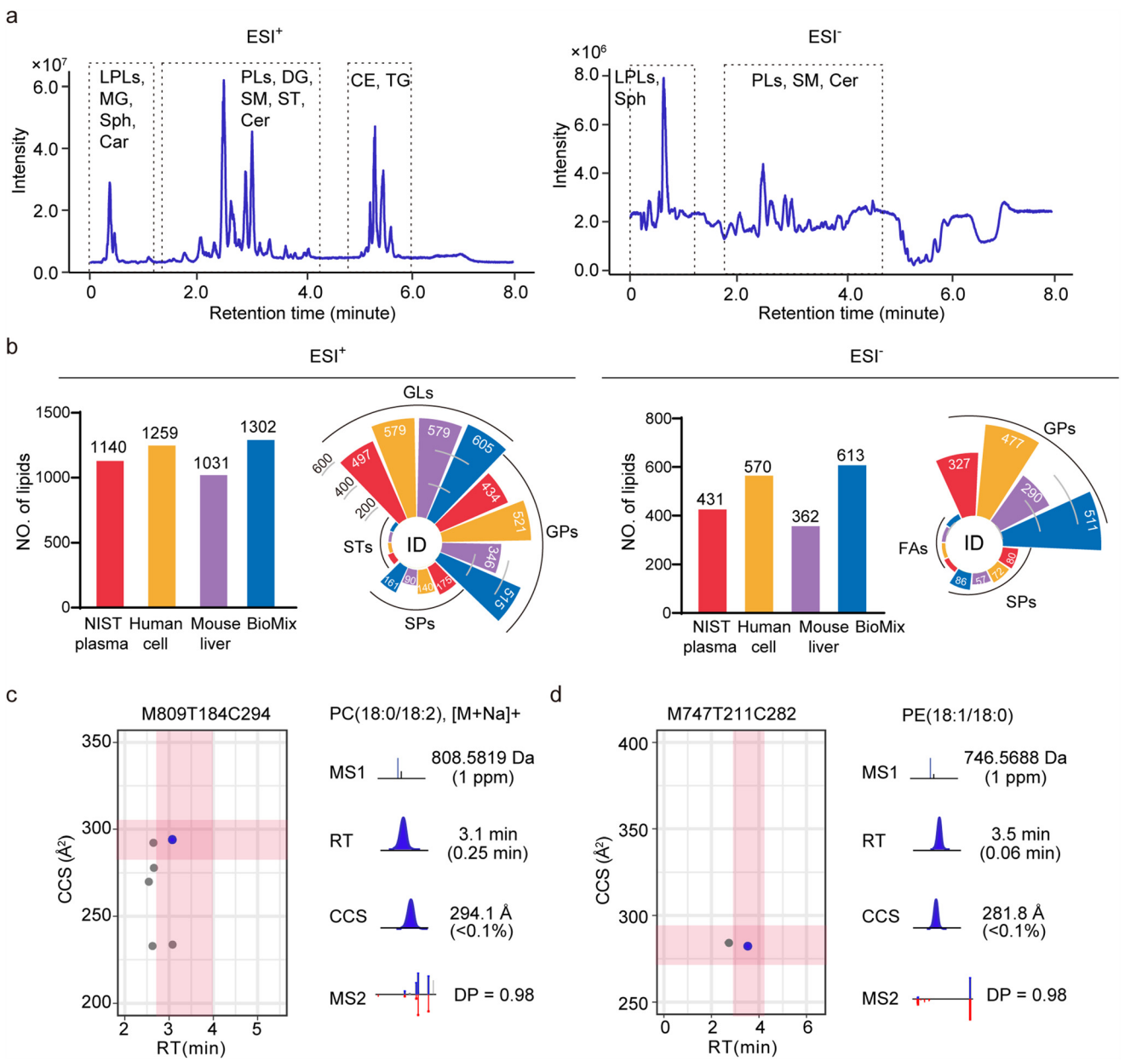

Fig. 3 The fast 4D lipidomics achieves the broad-coverage of distinct lipids in complex biological samples. (a) The base peak chromatogram (BPC) of the lipid extract from NIST human plasma (SRM 1950) in the positive ionization mode (left) and negative ionization mode (right), respectively. (b) Numbers of identified lipids in NIST human plasma, human cell (293T cells), mouse liver tissue, and the pooled biological mixture (BioMix) in the positive ionization mode (left) and negative ionization mode (right), respectively. $N = 6$ technical replicates in each analysis. (c and d) Identification of PC(18 : 0/18 : 2) (c) and PE(18 : 1/18 : 0) (d) in NIST human plasma through the four-dimensional library match. lysoPLs: lyso-phospholipids, MG: monoradylglycerols, Sph: sphinganine, Car: carnitines, PLs: phospholipids, DG: diacylglycerols, SM: sphingomyelins, ST: sterols, Cer: ceramides, CE: cholesteryl esters, TG: triglycerides, GLs: glycerolipids, GPs: glycerophospholipids, SPs: sphingolipids.

application using other types of biological samples, which includes human cell (293T cell), mouse liver, and the pooled mixture of NIST SRM 1950 plasma, human cell, and mouse liver. Specifically, 1140, 1250, and 1302 lipid species were identified in NIST SRM 1950 plasma, human cell, mouse liver, and pooled mixture using the positive ionization mode, respectively (Fig. 3b). Stratified by lipid categories, glycerolipids (GLs) are detected as the largest number of lipids in different biological samples ranging from 497 to 605 GL species, followed by the category of glycerophospholipids (GPs). 90 to 175 sphingolipids were measured in different complex matrices, while sterol lipids were less abundant (Fig. 3b). Notably, the identification results were reported as the lipid species level, fatty acyl level, or fatty acyl position level according to the curated fragmentation rules that we previously curated.[8] Results of data acquired in negative ionization mode are shown in Fig. 3a and b. The extracted ion chromatograms (EICs) of different lipid species are shown in ESI Fig. 2.† We further demonstrated the 4D identifications of PC (18 : 0/18 : 2) and PE (18 : 1/18 : 0) in NIST SRM 1950 plasma sample, respectively (Fig. 3c, d and ESI Fig. 3†). For PC (18 : 0/18 : 2) identification, six features were first putatively annotated with MS1-matched candidate (Fig. 2c). The addition of RT match, CCS match, and MS/MS spectral match further filtered false positives, and the feature M809T184C294 was finally annotated as PC (18 : 0/18 : 2). Likewise, the feature M747T211C282 was annotated as PE (18 : 1/18 : 0) through MS1 match, RT match, CCS match, and MS/MS spectral match with the 4D lipidomics strategy (Fig. 3d). Taken together, we demonstrated that the 8 min LC-IM-MS-based four-dimensional untargeted lipidomics enables the fast and comprehensive analysis of distinct lipids in complex biological matrices.

3.2 Quantification performances of the fast 4D lipidomics method

To evaluate the quantitative performances of the fast 4D lipidomics method, we spiked nine internal deuterated lipid standards in NIST human plasma and analyzed the plasma samples. Lipid species in the plasma were quantified with corresponding internal standards and calibration curves (ESI Table 2 and Fig. 4†). First, we assessed and demonstrated the linear ranges, the lower limit of detection (LOD), the lower limit of quantification (LOQ), and reproducibility among the replicates for individual lipid standards (ESI Table 4†). For NIST human plasma, we quantified a total of 836 lipid species from 13 lipid classes, with the lipid concentration ranging from 0.01 to 1000 nmol mL^{-1} (Fig. 4a). Furthermore, we validated the quantitative accuracy of the fast 4D lipidomics method by comparing the quantitative results with the values previously reported by 31 independent laboratories.[31] Using the LipidQC tool,[32] we compared the quantification results of 152 lipid species that were included in both LipidQC and our experiments. Among them, concentrations of 127 lipid species (83.5%) fell within the region of 99% confidence interval (Fig. 4b). In summary, the results demonstrated that the fast 4D untargeted lipidomics method enables to achieve accurate and high-throughput lipid quantifications for biological samples.

3.3 Lipidomic profiles of plasma from patients with colorectal cancers

To demonstrate the application of the fast 4D lipidomics method for clinical studies, we conducted the lipidomic profiling of plasma samples from a cohort of patients with CRC before and after surgery (*i.e.*, preoperative and postoperative plasma samples; Fig. 5a). The detailed information of the clinical cohort is listed in ESI Table 5.† In total, 1376 lipids were readily identified by MS1 accurate mass, RT, CCS, MS/MS spectral matches, and fragmentation rules using the 4D untargeted lipidomics strategy (Fig. 5b). Among them, 1110 lipids were quantified and subjected to further statistical analyses. Partial least square (PLS) analysis of the 4D untargeted lipidomics data revealed profound differences in the plasma lipidome before and after surgical operation (Fig. 5c). Subsequent univariate analysis showed that 115 lipid species were significantly changed between preoperative and postoperative plasma

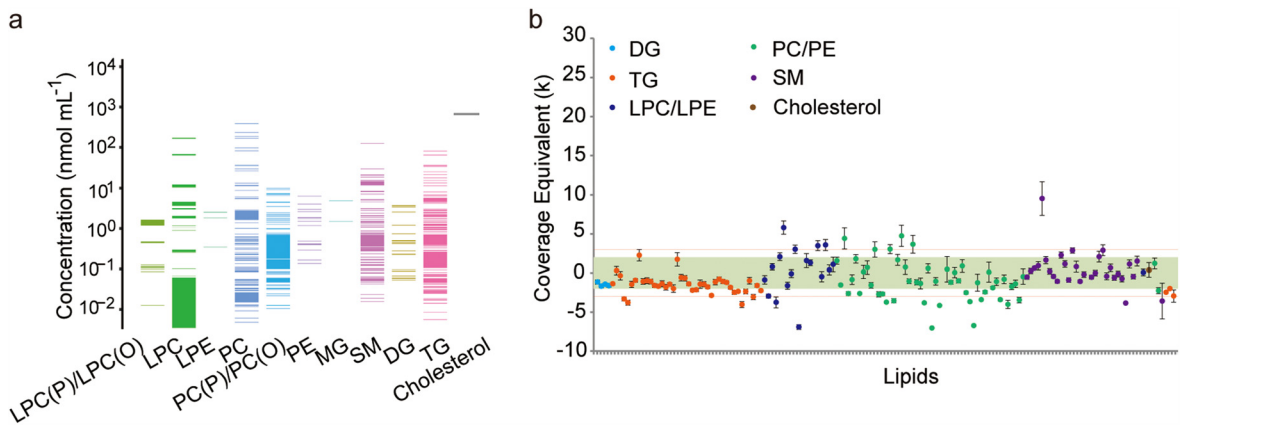

Fig. 4 Quantification performances of the fast 4D lipidomics method. (a) Quantified concentrations of the lipid species in NIST human plasma (SRM 1950). (b) Validation of the quantitation accuracy with the inter-laboratory reported values for NIST human plasma.

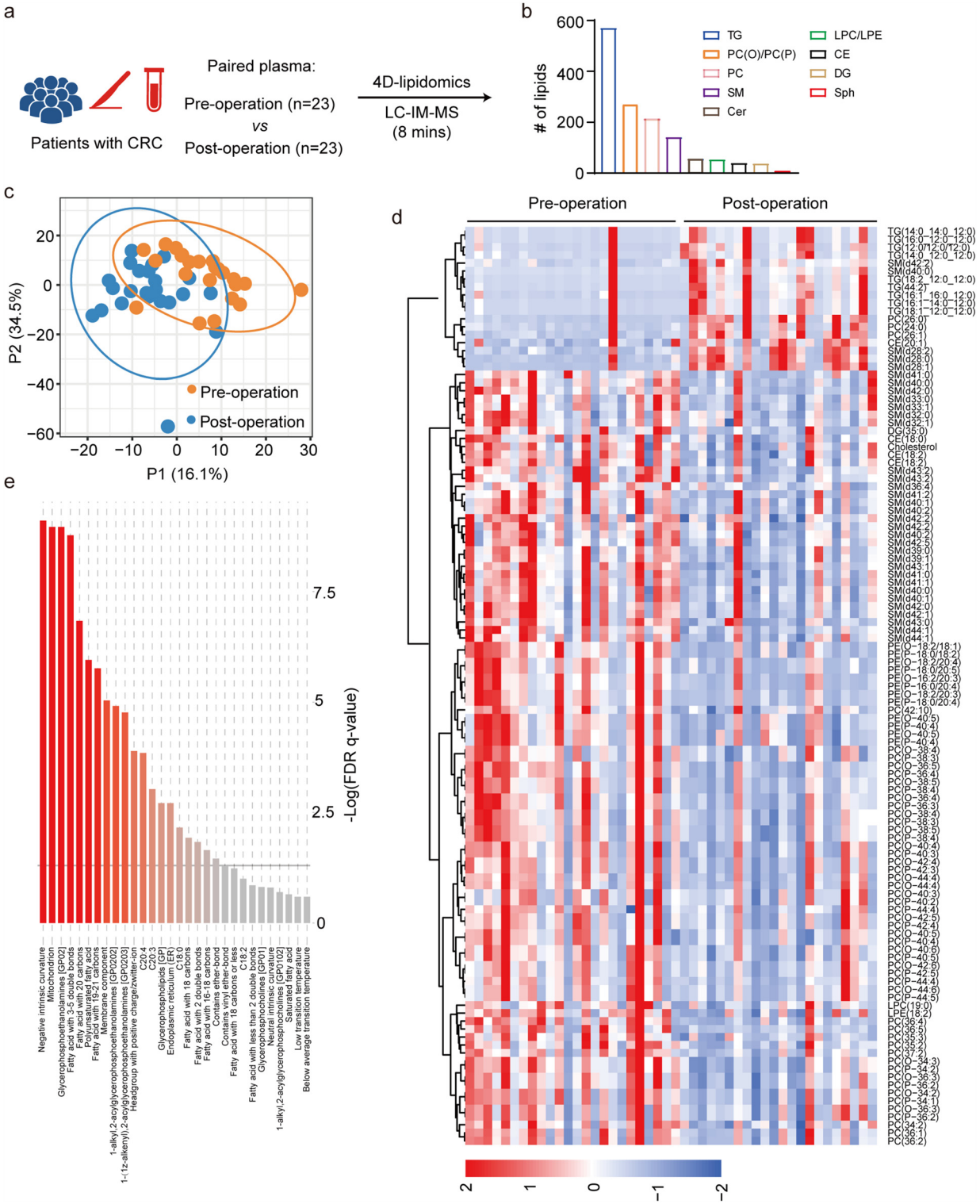

Fig. 5 Lipidomic profiles of plasma from patients with colorectal cancers. (a) The fast lipidomics analysis of plasma samples from a cohort of patients with CRC before and after surgery. (b) Numbers of identified lipids in each class in the plasma samples. (c) Supervised PLS plot for lipidomic profiles of preoperative and postoperative plasma of patients with CRC. (d) Heatmap for 115 significantly changed lipid species between preoperative and postoperative plasma. (e) Results of lipid ontology enrichment analysis using the LION tool.

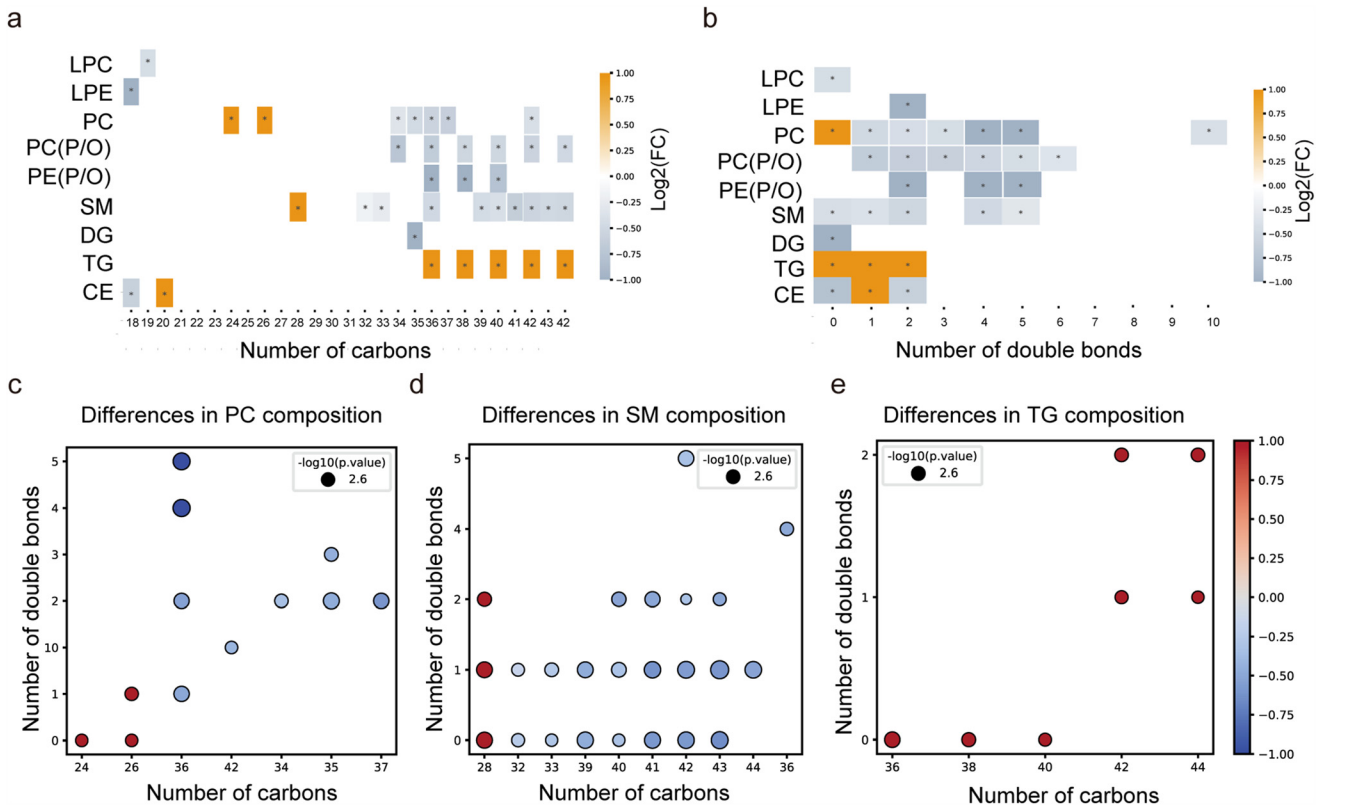

Fig. 6 Differences in carbon numbers and double bonds for lipid classes in patients with CRC. (a) Distribution of the number of carbons in significantly changed lipids for individual lipid classes. (b) Distribution of the number of double bonds in significantly changed lipids for individual lipid classes. Bubble plots illustrate compositional changes in (c) PCs, (d) SMs, and (e) TGs. Lipids were classified according to the total carbon atom numbers and number of double bonds. The bubble size represents the sum of all lipid species (with different acyl compositions) that contained the defined total carbon atom numbers and total double bond numbers.

(Fig. 5d). Phosphatidylcholines (PCs) and phosphoethanolamines (PE) were found as significantly decreased in the postoperative plasma of patients after surgery, while a fraction of triglycerides (TGs) was increased. Furthermore, the 4D lipidomic profiles were then applied to the lipid ontology enrichment analysis using the LION tool.[33] The ontology terms were evaluated using the analysis of variance values in the significantly changed lipids. The results revealed significant enrichment in negative intrinsic curvature, mitochondrion, glycerophosphoethanolamines, distinct fatty acid classes, and so on (Fig. 5e). Also, ontologies associated with membrane component and endoplasmic reticulum were significantly enriched. This enrichment result was in line with previous studies that reported that essential components of cell membranes such as phosphatidylcholines (PCs) and lysophosphatidylcholines (LPCs) were associated with CRC formation.[34,35]

Given the dysregulation in the above lipid classes, we further investigated the variations in carbons and double bonds within these lipid molecules between preoperative plasma and postoperative plasma from patients with CRC. The majority of down-dysregulated lipid classes including PC, PC (P/O), PE(P/O), and SM were found to carry carbons longer than 32 (Fig. 6a and ESI Fig. 5†). As for the results of unsaturation investigation, we found that dysregulated lipids predominantly had less than five double bonds in total (Fig. 6b). The results of exemplar lipid classes including PC, SM, and TG are demonstrated in Fig. 6c–e. Specifically, the levels of saturated PC lipids with C24 to C26 and monounsaturated PCs with C26 were significantly elevated in postoperative plasma, while the rest of PC lipids were decreased (Fig. 6c). Similarly, the levels of SM lipids with C28 were up-regulated and the others were down-regulated in postoperative plasma (Fig. 6d). On the other hand, up-regulated TG lipids were observed in postoperative plasma regarding either the number of carbons or double bonds (Fig. 6e).

4. Conclusions

Lipidomics enables to comprehensively measure complex lipids with a broad-coverage and provides a holistic understanding of the lipid metabolism. Leveraged by the fast separation of ion mobility, we developed a fast LC-IM-MS method (8 minutes) towards high-throughput untargeted lipidomics, wherein the four-dimensional information on m/z of MS1, retention time, CCS, and MS/MS spectra can be acquired sim-

ultaneously in one analysis. The 4D untargeted lipidomics strategy is supported by 4D untargeted lipidomics data processing, which integrates IM-MS-based 4D peak detection and 4D lipid identification. The fast LC-IM-MS method not only detected over 1000 lipid molecules in a single analysis but also achieved accurate quantifications for a broad-coverage of lipids in biological samples. In addition, the 8 minute LC-IM-MS method exhibited extremely high reproducibility with respect to the measured mass accuracy, retention time, CCS, and lipid abundances, which is highly suitable for the lipidomic analyses of large-scale clinical samples. A practical application of the method was demonstrated using a cohort of plasma samples for patients with CRC. We believe that this fast and broad-coverage lipidomics method will be widely used in distinct application scenarios, particularly for large-scale clinical lipidomic studies.

Author contributions

Zheng-Jiang Zhu: conceptualization, funding acquisition, review and editing, investigation. Yuping Cai: conceptualization, methodology, data analysis, and writing. Xi Chen: conceptualization, data acquisition. Fandong Ren: sample preparation, data acquisition. Hongmiao Wang: data analysis. Yandong Yin: data analysis.

Data availability

The data supporting this article have been included as part of the ESI figures and table.†

Conflicts of interest

There are no conflicts to declare.

Acknowledgements

The work was supported by National Key R&D Program of China (2018YFA0800902), Science and Technology Commission of Shanghai Municipality (21JC1405902), Shanghai Key Laboratory of Aging Studies (19DZ2260400), Shanghai Municipal Science and Technology Major Project, and Shanghai Basic Research Pioneer Project.

References

1 M. T. Snaebjornsson, S. Janaki-Raman and A. Schulze, *Cell Metab.*, 2020, **31**, 62–76.
2 H. Prendeville and L. Lynch, *Cell. Mol. Immunol.*, 2022, **19**, 432–444.
3 C. W. Ko, J. Qu, D. D. Black and P. Tso, *Nat. Rev. Gastroenterol. Hepatol.*, 2020, **17**, 169–183.
4 H. Miao, B. Li, Z. Wang, J. Mu, Y. Tian, B. Jiang, S. Zhang, X. Gong, G. Shui and S. M. Lam, *Research*, 2023, **6**, 0185.
5 M. R. Wenk, *Cell*, 2010, **143**, 888–895.
6 X. Han, *Nat. Rev. Endocrinol.*, 2016, **12**, 668–679.
7 Y. H. Rustam and G. E. Reid, *Anal. Chem.*, 2018, **90**, 374–397.
8 X. Chen, Y. Yin, M. Luo, Z. Zhou, Y. Cai and Z. J. Zhu, *Anal. Chim. Acta*, 2022, **1210**, 339886.
9 T. Cajka and O. Fiehn, *TrAC, Trends Anal. Chem.*, 2014, **61**, 192–206.
10 M. Holcapek, G. Liebisch and K. Ekroos, *Anal. Chem.*, 2018, **90**, 4249–4257.
11 L. Novakova, P. Chocholous and P. Solich, *Talanta*, 2014, **121**, 178–186.
12 J. Tu, Z. Zhou, T. Li and Z.-J. Zhu, *TrAC, Trends Anal. Chem.*, 2019, **116**, 332–339.
13 C. Hinz, S. Liggi and J. L. Griffin, *Curr. Opin. Chem. Biol.*, 2018, **42**, 42–50.
14 R. A. Harris, K. L. Leaptrot, J. C. May and J. A. McLean, *TrAC, Trends Anal. Chem.*, 2019, **116**, 316–323.
15 Z. Zhou, X. Shen, J. Tu and Z. J. Zhu, *Anal. Chem.*, 2016, **88**, 11084–11091.
16 Z. Zhou, M. Luo, X. Chen, Y. Yin, X. Xiong, R. Wang and Z. J. Zhu, *Nat. Commun.*, 2020, **11**, 4334.
17 X. Zheng, R. D. Smith and E. S. Baker, *Curr. Opin. Chem. Biol.*, 2018, **42**, 111–118.
18 K. L. Leaptrot, J. C. May, J. N. Dodds and J. A. McLean, *Nat. Commun.*, 2019, **10**, 985.
19 M.-D. Luo, Z.-W. Zhou and Z.-J. Zhu, *J. Anal. Test.*, 2020, **4**, 163–174.
20 J. E. Kyle, X. Zhang, K. K. Weitz, M. E. Monroe, Y. M. Ibrahim, R. J. Moore, J. Cha, X. Sun, E. S. Lovelace, J. Wagoner, S. J. Polyak, T. O. Metz, S. K. Dey, R. D. Smith, K. E. Burnum-Johnson and E. S. Baker, *Analyst*, 2016, **141**, 1649–1659.
21 G. Paglia, M. Kliman, E. Claude, S. Geromanos and G. Astarita, *Anal. Bioanal. Chem.*, 2015, **407**, 4995–5007.
22 Z. Zhou, J. Tu, X. Xiong, X. Shen and Z. J. Zhu, *Anal. Chem.*, 2017, **89**, 9559–9566.
23 H. Zhang, M. Luo, H. Wang, F. Ren, Y. Yin and Z. J. Zhu, *Anal. Chem.*, 2023, **95**, 13913–13921.
24 E. S. Baker, W. Uritboonthai, A. Aisporna, C. Hoang, H. M. Heyman, L. Connell, D. Olivier-Jimenez, M. Giera and G. Siuzdak, *Nat. Metab.*, 2024, **6**, 981–982.
25 X. Chen, Y. Yin, Z. Zhou, T. Li and Z. J. Zhu, *Anal. Chim. Acta*, 2020, **1136**, 115–124.
26 M. Luo, Y. Yin, Z. Zhou, H. Zhang, X. Chen, H. Wang and Z. J. Zhu, *Nat. Commun.*, 2023, **14**, 1813.
27 C. G. Vasilopoulou, K. Sulek, A. D. Brunner, N. S. Meitei, U. Schweiger-Hufnagel, S. W. Meyer, A. Barsch, M. Mann and F. Meier, *Nat. Commun.*, 2020, **11**, 331.
28 Z. Wang, B. Cui, F. Zhang, Y. Yang, X. Shen, Z. Li, W. Zhao, Y. Zhang, K. Deng, Z. Rong, K. Yang, X. Yu, K. Li, P. Han and Z. J. Zhu, *Anal. Chem.*, 2019, **91**, 2401–2408.
29 V. Matyash, G. Liebisch, T. V. Kurzchalia, A. Shevchenko and D. Schwudke, *J. Lipid Res.*, 2008, **49**, 1137–1146.

30 J. Tu, Y. Yin, M. Xu, R. Wang and Z. J. Zhu, *Metabolomics*, 2017, **14**, 5.
31 J. A. Bowden, A. Heckert, C. Z. Ulmer, C. M. Jones, J. P. Koelmel, L. Abdullah, L. Ahonen, Y. Alnouti, A. M. Armando, J. M. Asara, T. Bamba, J. R. Barr, J. Bergquist, C. H. Borchers, J. Brandsma, S. B. Breitkopf, T. Cajka, A. Cazenave-Gassiot, A. Checa, M. A. Cinel, R. A. Colas, S. Cremers, E. A. Dennis, J. E. Evans, A. Fauland, O. Fiehn, M. S. Gardner, T. J. Garrett, K. H. Gotlinger, J. Han, Y. Huang, A. H. Neo, T. Hyotylainen, Y. Izumi, H. Jiang, H. Jiang, J. Jiang, M. Kachman, R. Kiyonami, K. Klavins, C. Klose, H. C. Kofeler, J. Kolmert, T. Koal, G. Koster, Z. Kuklenyik, I. J. Kurland, M. Leadley, K. Lin, K. R. Maddipati, D. McDougall, P. J. Meikle, N. A. Mellett, C. Monnin, M. A. Moseley, R. Nandakumar, M. Oresic, R. Patterson, D. Peake, J. S. Pierce, M. Post, A. D. Postle, R. Pugh, Y. Qiu, O. Quehenberger, P. Ramrup, J. Rees, B. Rembiesa, D. Reynaud, M. R. Roth, S. Sales, K. Schuhmann, M. L. Schwartzman, C. N. Serhan, A. Shevchenko, S. E. Somerville, L. St John-Williams, M. A. Surma, H. Takeda, R. Thakare, J. W. Thompson, F. Torta, A. Triebl, M. Trotzmuller, S. J. K. Ubhayasekera, D. Vuckovic, J. M. Weir, R. Welti, M. R. Wenk, C. E. Wheelock, L. Yao, M. Yuan, X. H. Zhao and S. Zhou, *J. Lipid Res.*, 2017, **58**, 2275–2288.
32 C. Z. Ulmer, J. M. Ragland, J. P. Koelmel, A. Heckert, C. M. Jones, T. J. Garrett, R. A. Yost and J. A. Bowden, *Anal. Chem.*, 2017, **89**, 13069–13073.
33 M. R. Molenaar, A. Jeucken, T. A. Wassenaar, C. H. A. van de Lest, J. F. Brouwers and J. B. Helms, *GigaScience*, 2019, **8**, giz061.
34 A. Mika, A. Pakiet, A. Czumaj, Z. Kaczynski, I. Liakh, J. Kobiela, A. Perdyan, K. Adrych, W. Makarewicz and T. Sledzinski, *J. Clin. Med.*, 2020, **9**, 1095.
35 T. Salita, Y. H. Rustam, D. Mouradov, O. M. Sieber and G. E. Reid, *Cancers*, 2022, **14**, 3714.